ACS APPLIED MATERIALS & INTERFACES

Research Article

www.acsami.org

Micropatterned Stretchable Circuit and Strain Sensor Fabricated by Lithography on an Electrospun Nanofiber Mat

Minwoo Park,[†] Jungkyun Im,[‡] JongJin Park,*[,‡] and Unyong Jeong*[,†]

[†]Department of Materials Science and Engineering, Yonsei University, 134 Shinchon-dong, Seoul, Korea

[‡]Samsung Advanced Institute of Technology, Mt.14-1, Nongseo-Dong, Giheung-Gu,Yongin-Si, Gyeonggi-Do 446-712, Korea

Supporting Information

ABSTRACT: This paper describes a novel approach for composite nanofiber mats and its application to fabricate a strain sensor. Electrospun poly(4-vinylpyridine) (P4VP) nanofiber mats are micropatterned by a lithographic approach that includes selective oxidation of the nanofibers and removal of unreacted fibers. The P4VP/$HAuCl_4$ complex is converted to P4VP/Au composites by chemical reduction. We investigate the electrical resistivity of the composite mats according to the number of complexation-and-reduction cycles, the thickness of the fiber mats, and the annealing temperatures which control the percolation of the Au nanoparticles in the fiber mats. Nozzle printing of a polymeric solution on the patterned nanofiber mats simply produces an array of strain-sensitive and strain-invariant units. The patterns demonstrate high strain-sensing performance without any mechanical and electrical failure over 200 bending cycles in the strain range of $\varepsilon < 0.17$.

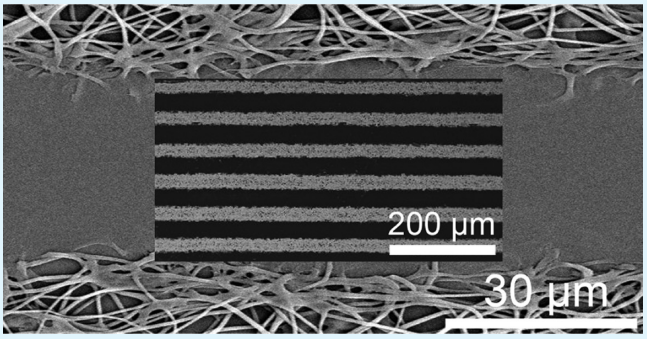

KEYWORDS: *stretchable electronics, strain sensors, nanofiber, electrospinning, micropatterning, nanocomposites*

INTRODUCTION

Stretchable, conductive materials have been of great interest because they are essential elements to realize deformable electronics. A substance with a high conductivity and electrical stability at large strains can be used to constitute stretchable circuits and interconnects.[1,2] A material whose electrical properties change sensitively to external stimuli is useful to fabricate sensors recognizing the change of strain, pressure, temperature, and chemicals.[3−7] Metal stripes with a wavy geometry,[8,9] liquid metals,[10] and elastomer composites with Ag nanowires[11,12] can afford mechanical durability and metallic conductivity at large strains, hence they are suitable to electric circuits. Rubber composites embedding carbon nanotubes or metal nanoparticles have been exploited to sense the strains applied to an elastomer substrate.[13,14] Micropattern fabrication of those materials on a stretchable substrate is a prerequisite for integrated deformable devices. The process to obtain micropatterned metal stripes is well-established and has been successfully employed in stretchable displays and transistors.[15,16] However, patterning the other materials in micrometer scale has not been successfully demonstrated so far and remains a challenging subject to be accomplished.

Very recently, we demonstrated a highly stretchable circuit made of electrospun rubber composite nanofibers with Ag nanoparticles.[17] The curved geometry of the nanofibers prevented accumulation of the stress in the nanofibers even at large strains ($\varepsilon = 0.6$), which enabled retention of the high conductivity at large strains. The result indicates that micropatterning a mat of composite nanofibers, if possible, can be a good strategy to obtain conductive stretchable circuits or strain sensors. Several papers have reported the nanofiber-based strain sensors fabricated by electrospinning. A nanofiber mat of ferroelectric polymer, poly(vinylidenefluoride-*co*-trifluoroethylene), was used for strain sensing that was dependent on the direction of strain.[18] Composite nanofibers consisting of carbon black particles and poly(ε-caprolactone) showed a reliable strain sensing.[19] Very recently, polystyrene nanofibers on which ZnO nanowires grew densely in the radial direction of the nanofibers showed a high sensitivity for uniaxial stretching.[20] In this paper, we introduce a facile approach to generate an arbitrary micropattern of a conductive stretchable composite mat. The conductivity of the pattern is controllable; hence we demonstrate an array of high-performance strain sensors whose circuits and sensing units are fabricated simultaneously by the same composite mats with different conductivities.

Major interest in electrospinning has been focused on the bulk properties of nanofiber mats that do not require micropatterning. Several methods have been suggested to produce patterned nanofiber mats. A variety of fiber patterns were produced by employing microcontact printing and photolithography.[21] As an another approach for patterning, direct UV-assisted patterning was demonstrated on the nanofiber mat which was electrospun from a polymer solution

Received: July 2, 2013
Accepted: August 19, 2013
Published: August 19, 2013

   dx.doi.org/10.1021/am4026032 | *ACS Appl. Mater. Interfaces* 2013, 5, 8766−8771

containing a UV cross-linker.[22] In conventional methods, nanofibers are collected in an aligned fashion by adjusting the electric field of a collector[23] or by employing a rotating collector.[24] However, these methods can be used to obtain patterns on the millimeter scale. Recent attempts to use nanofibers for electronic devices[25] have required the fabrication of micropatterns. Near-field electrospinning has been developed to obtain linear patterns made of a single nanofiber.[26] In order to fabricate arbitrary patterns without compromising on the advantages of electrospinning (easy and large-scale production), a new method for patterning nanofiber mats is required. We speculate that the arbitrary micropatterning of electrospun nanofiber mats may be achieved in three ways: (i) direct printing of target materials on a nanofiber mat, (ii) coating a protection layer on a mat and removing other materials, and (iii) direct etching of a selected area to obtain a patterned nanofiber mat on a substrate. The validity of the first approach was proved by the rubber composite nanofibers mentioned above.[17] The second approach was demonstrated by embedding poly(3-hexylthiophene) nanofibers in a hydrogel pattern.[27] For obtaining the desired pattern resolution, this study introduces a lithographic approach as the third method. A pattern is created by exposing an electrospun poly(4-vinlypyridine) (P4VP) nanofiber mat to UV/O_3 (UVO) radiation through a metallic mask, which oxidized the nanofibers. The nanofibers shielded by the mask were dissolved in a solvent in an analogy with conventional photolithography.

EXPERIMENTAL SECTION

Materials. Poly(4-vinlypyridine) (P4VP, M_w = 160 000), polystyrene (PS, M_w = 350 000), gold chloride trihydrate ($HAuCl_4 \cdot 3H_2O$, 99.9%), hydrazine hydrate (N_2H_4, 50−60%), and EGaIn (Ga−In eutectic, 99.99%) were purchased from Sigma Aldrich. *N*,*N*-Dimethylformamide (DMF, 99.9%), ethanol (95.0%), and chloroform (99.9%) were purchased from J.T. Baker. A 50 μm line-and-space Ni photomask was fabricated by laser patterning (thickness, 50 μm; pattern length, 1.5 cm).

Patterning of P4VP Nanofibers. P4VP of 30 wt % was dissolved in DMF at 50 °C. The solution was injected at 10 μL/min. The applied voltage was 12.0 kV, and the nozzle-to-collector distance was 15 cm. Electrospun nanofibers were collected on a PET film. A Ni shadow mask was placed on the nanofiber mat, and the mat was then irradiated with UVO for 10 min. The nanofibers shielded by the mask were immediately dissolved in ethanol.

Fabrication of Composite Mat and Strain Sensors. A gold precursor ($HAuCl_4 \cdot 3H_2O$) was dissolved in 0.02 M ethanol. The patterned nanofiber mat was dipped in the precursor solution for 1 min, and was then dipped in pure water to remove the precursors that did not coordinate with the pyridyl groups. N_2H_4 was diluted (10%, v/v) in ethanol, and three to four drops were placed in a Petri dish. The Au-coordinated fiber specimens were put in the Petri dish for 5 min to convert the Au precursors into Au nanoparticles. The residual N_2H_4 vapor was rinsed out several times by using deionized water. This process was repeated twice for the strain-sensitive part and thrice for the strain-invariant conductive circuit. In order to fabricate the strain sensor, a PS solution (15 wt % in chloroform) was nozzle-printed (SHOTMASTER 300, Musashi Engineering) at the center of the fiber pattern. An air pressure of 100 kPa was applied for the printing.

Bending Test. Small droplets of EGaIn (Ga−In eutectic liquid metal) were put on the edges of conductive composite circuits on the PET film. A marginal area of the PET substrate was inserted in metallic bars of a bending machine. Glass slides were put between the metal bar and specimen to maintain the symmetry of the PET substrate. Al wires connected to the liquid metal drop were wrapped around the bars and connected to a Keithley SourceMeter. The bending frequency was one cycle per second.

Characterization. Fourier transform infrared spectroscopy (FT-IR) analysis was conducted in ATR mode (Vertex 70, Bruker). Scanning electron microscopy (SEM) images and energy-dispersive X-ray (EDX) data were taken by field-emission SEM (FE-SEM, JSM-7001F, JEOL). Dark-field scanning transmission electron microscopy (STEM) and high resolution TEM (HR-TEM) images were taken by using Tecnai F20ST (FEI. Co.) and JEOL 2100F instruments, respectively. Resistance of the P4VP/Au nanofiber mats was measured by Agilent 4156A. Resistance changes according to the strain versus time were obtained by a stretching/bending tester (Z-tec. Co.) and a Keithley SourceMeter 2500 (keithley Instrument. Inc.). Stress−strain curves were obtained using a tensile stress tester (Linkam Scientific Instruments).

RESULTS AND DISCUSSION

Figure 1 displays the color changes during the process for a conductive P4VP/Au composite nanofiber mat. First, A P4VP nanofiber mat was obtained by electrospinning and it was oxidized by UVO treatment. Immersion of the mat into a Au precursor solution induced the complexation of P4VP and Au precursors. Chemical reduction of Au precursors generated Au nanoparticles that were percolated on the fibers, which showed an electrically conductive mat. Figure 1A and B shows a photograph of the oxidized P4VP nanofiber mat and its magnified SEM image, respectively. The color of the mat changed from white to bright yellow (Figure 1A), and no noticeable change in the fiber morphology of the mat was observed (Figure 1B). The oxidation of P4VP chains changed their molecular structure so that they were insoluble in the ethanol precursor solution, which enabled solution process to produce the composite mat. The complexation of P4VP and $HAuCl_4$ was progressed in an ethanol solution. It resulted in the color change of the mat from bright yellow to dark yellow (Figure 1C). After washing the excess precursors, Au nanoparticles were synthesized through chemical reduction of the precursor. The repeated complexation-and-reduction cycles increased the number density of the Au nanoparticles. They changed the color of the mat from dark blue to brown as depicted in Figure 1C.

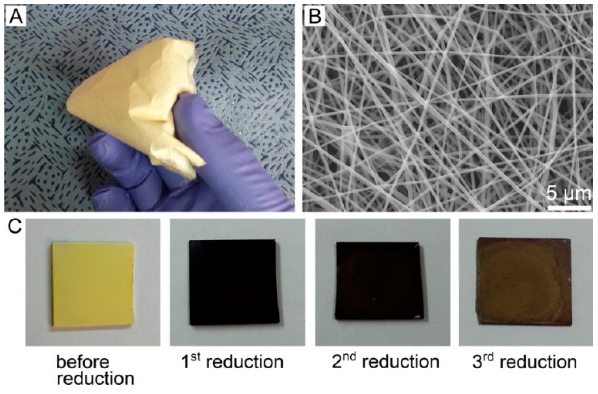

Figure 1. Electrospun P4VP nanofiber mat oxidized through UV/O_3 (UVO) exposure and its composite with Au nanoparticles obtained by complexation-and-reduction cycles. (A) Photograph of the oxidized P4VP nanofiber mat. (B) SEM image of the nanofibers after UVO treatment. (C) Sequential photographs according to the number of complexation-and-reduction cycles of the oxidized P4VP nanofiber mat.

Figure 2 shows the stress−strain curves obtained from three samples; the pristine P4VP fiber mat, the oxidized P4VP fiber mat, and the P4VP/Au composite fiber mat. The specimens

dx.doi.org/10.1021/am4026032 | ACS Appl. Mater. Interfaces 2013, 5, 8766−8771

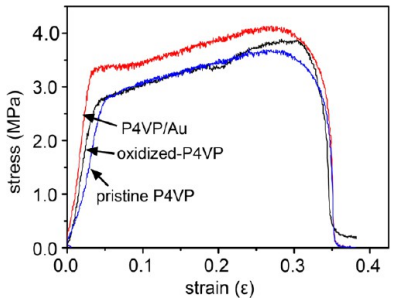

Figure 2. Stress–strain curves for three samples: pristine P4VP fiber mat (blue line), oxidized P4VP fiber mat (black line), and P4VP/Au composite fiber mat (red line).

were prepared by cutting a large uniform nanofiber mat. The dimension of the samples was identical, 5 mm in width, 30 mm in length, and 20 μm in thickness. Constant tensile force (20 N) with 20 μm/s was applied until ε = 0.37 at which the samples were torn apart. The overall shapes of the stress–strain curves were almost the same, and the samples had the same yield strain. It indicates that the nanofiber mat maintained its overall mechanical behavior. Young's modulus (E) increased slightly from 55 MPa for the pristine mat to 95 MPa for the oxidized mat and to 136 MPa for the P4VP/Au composite mat. The modulus of P4VP/Au composite mat increased by 43% in comparison with the oxidized mat, which is similar to the report from a composite fiber mat containing Ag nanoparticles.[17]

Figure 3 exhibits the patterning of electrospun P4VP nanofibers by the selective oxidation process. The nanofibers

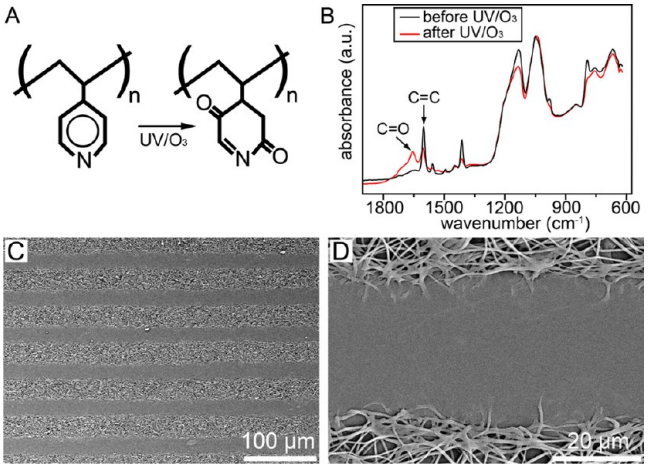

Figure 3. Lithographic micropatterning of electrospun P4VP nanofibers. (A) Molecular change in P4VP by UVO treatment. (B) FT-IR analysis before and after UVO exposure of the P4VP nanofiber mat. The black and red lines indicate the as-spun P4VP nanofiber mat and oxidized nanofibers, respectively. C=O stretching in modified pyridyl groups is represented by the peak at 1651.0 cm^{-1}. (C) SEM image of the nanofiber pattern obtained after UVO exposure through a 30-μm line-and-space Ni mask, followed by dissolving the nanofibers shielded by the mask. (D) Magnified SEM image of (C), indicating no residual nanofibers on the PET film.

(diameter: 150–400 nm) were collected on a Si wafer, a PET film and a glass slide. The nanofiber mat was exposed to UVO (28 mW/cm^2, AHTECH LTS) for 10 min. The highly reactive oxygen radicals converted the C=C bonds of pyridyl groups into carbonyl groups (Figure 3A). The conversion was confirmed by FT-IR spectroscopy in the attenuated total reflection (ATR) mode (Figure 3B). For drying the solvent completely, the as-spun fiber mat (thickness: 50 μm) was kept in vacuum for 12 h before the FT-IR analysis. Absorbance of the C=C stretching at 1598.9 cm^{-1} from the as-spun mat significantly decreased and a peak corresponding to the C=O stretching emerged at 1651.0 cm^{-1}. The P4VP nanofibers were soluble in ethanol, while the oxidized nanofibers were not. This difference in solubility enabled lithographic patterning of the mat by exposing it to UVO through a metal mask. Figure 3C shows a SEM image of a 30-μm-wide line pattern. The P4VP nanofiber mat was covered with a Ni mask with a line-and-space resolution of 30 μm and was then exposed to UVO for 10 min. The shielded area was clearly washed out by dipping it in ethanol, while the oxidized nanofiber pattern remained intact. The depth of oxidation in a P4VP film on a Si wafer was found to be about 500 nm for 3 min UVO treatment. It indicates that nanofibers thinner than 1 μm can be oxidized fully, hence there is no bottom limit in the nanofiber thickness. For the thicker nanofibers, the oxidized layer at the surface can protect dissolution of the polymer in the core. Therefore, thick nanofibers can be patterned by this technique in spite of their partial oxidation by UVO treatment. Figure 3D shows a magnified SEM image of the clear area between the line patterns. The nanofibers at the edge of the pattern were hung a bit to the dissolved area because of the leakage of oxygen radicals during the UVO treatment; however, there were no connections or residual nanofibers in the area.

Because ozone of the UVO is diffusive in the mat, the oxidation of fiber mat has a gradient from the edges of the mask pattern. Therefore, the resolution of the pattern becomes low as the thickness of the mat is increased. The permeation limit of the reactive oxygen was about 20 μm in the nanofiber mat. The diffusion of the reactive oxygen was found to be about 1.5 μm from the edges of the mask pattern for the 20-μm-thick mat. We suppose the diffusion length of the reactive oxygen is not considerable for a mat of nanofiber monolayer. For example, if the nanofibers are 300-nm-thick and they are aligned to form a monolayer, the resolution through this approach can be very close to the resolution of the mask.

The pyridyl group in P4VP forms complexes with metal precursors when they are protonated in solutions. Figure 4A shows a schematic of the complexation process between a Au

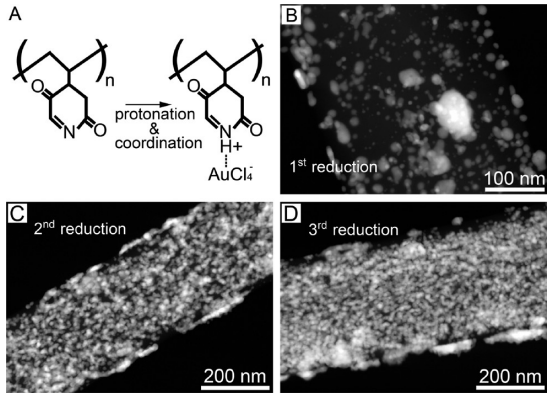

Figure 4. Deposition of Au nanoparticles on oxidized P4VP nanofibers. (A) Coordination of $AuCl_4^-$ to the pyridyl group of P4VP. (B–D) Dark-field STEM images of P4VP/Au composite nanofibers obtained after the first, second, and third reduction cycles.

dx.doi.org/10.1021/am4026032 | ACS Appl. Mater. Interfaces 2013, 5, 8766–8771

precursor and an oxidized P4VP nanofiber. Several reports have already demonstrated composite nanofibers obtained through complexation between P4VP and Au precursors.[28,29] In this study, the complexing characteristics of P4VP were utilized together with the patterning of the nanofiber mat. For reducing the precursor into metal nanoparticles, electroless plating has been widely used. The pyridyl group was protonated in the solution ($N-H^+$) and strongly attracted the $AuCl_4^-$ anions by electrostatic interactions.[30] This process takes a long time for the percolation of metal nanoparticles owing to the slow reduction of the precursor by the electrons donated by nitrogen. Therefore, instead of electroless plating, we employed a process involving repeated complexation−rinse−reduction for quick composite formation. The patterned nanofiber mat on a substrate was dipped in a Au precursor solution (0.02 M $HAuCl_4 \cdot 3H_2O$ in ethanol) for 1 min. The specimen was immersed for a short time in water to rinse the excess precursor that did not coordinate with the polymer chains. The nanofiber mat was then taken out of the solution, dried in air, and reduced in a chamber by using a strong reducing agent, vaporized hydrazine hydrate ($N_2H_4 \cdot 3H_2O$).[31,32] Vaporized hydrazine effectively penetrated each nanofiber and quickly reduced the precursor. The conductivity of the nanofiber mat increased with the reaction time and saturated after 5 min, which was regarded as the completion time for the reduction process. The composite nanofibers were thoroughly rinsed by dipping in deionized water to remove any residual hydrazine hydrate. The pyridyl groups in the P4VP fibers could form a complex with the Au precursors again during the second dipping. This allowed repeated cycles of the complexation−rinse−reduction process. Figure 4B−D shows high-angle annular dark-field STEM (HAADF-STEM) images of the nanofiber mat after the first, second, and third cycles. We examined the atomic percentage of the Au nanoparticles on the nanofiber surfaces by EDX spectroscopy. The average atomic percentages of Au nanoparticles were 9.5, 35.7, and 53.3%, in that order. The Au nanoparticles on the nanofibers had a broad size distribution (2−30 nm) and had the face-centered cubic (fcc) crystal structure (Figure S1, Supporting Information).

The increase in the number density of the nanoparticles allowed electrical percolation. The resistivity of the nanofiber mat depended on its thickness (t) as well as on the number of reduction cycles (Figure 5A). The resistivity (ρ) of the nanofiber mat was calculated using the equation,[33] $\rho = R(Wt)/L$, where R is the resistance of the mat, L is the distance between the two probe tips, and W is the width of the mat. The values of L (1 cm) and W (0.5 cm) were same for all samples. Because the fiber mat was collected on a flat moving stage, thickness of the mat was uniform (deviation ~ ±1 μm). We measured the thickness of the mat with cross-sectional SEM images taken at typically 10 different positions. The resistivity of the mat steadily decreased with an increase in its thickness; this was due to an increase in the number of current paths along the thickness direction.[17] The resistivity became saturated at t = 20 μm. After the first reduction cycle, the resistivity was 4.23×10^5 Ω·cm at t = 2 μm and 3.22×10^4 Ω·cm at t = 20 μm. Electrical percolation was achieved after the second reduction cycle, and the resistivity dropped to 2.56 Ω·cm at t = 2 μm and 4.57×10^{-1} Ω·cm at t = 20 μm. After the third reduction cycle, the resistivity of the nanofiber mat showed a further significant decrease, dropping to 2.32×10^{-2} Ω·cm at t = 2 μm and 2.4×10^{-3} Ω·cm at t = 20 μm. Subsequent reduction cycles did not cause any change in the resistivity, indicating saturated percolation of the nanoparticles. The number of the binding sites decreases as the number of reduction cycle increases because the Au nanoparticles on the surfaces hinder the binding of Au ions. We found that the additional binding of Au ions is negligible after the third reduction cycle, so the resistivity becomes saturated.

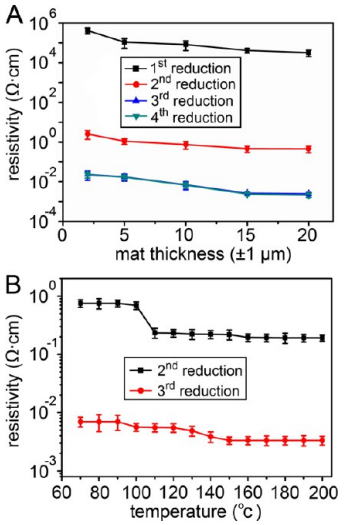

Figure 5. Effect of thickness (t) and thermal annealing on the resistivity of P4VP/Au composite nanofiber mats. (A) Resistivity changes according to the thickness of the nanofiber mat. The first, second, third, and fourth reduction indicate the number of reduction cycles. The resistivities after the third and fourth reductions overlapped for all thickness values. (B) Resistivity changes according to annealing temperature for patterned nanofiber mats (t = 10 μm) after the second and third reduction cycles.

The resistivity of the fiber mat could be reduced by thermal annealing. Figure 5B exhibits the effect of annealing on the resistivity of the nanofiber mat with t = 10 μm. The annealing temperature was increased from 70 to 200 °C in 10 °C steps with 5 min measuring time. The resistivity after the second reduction cycle decreased from 7.5×10^{-1} to 1.9×10^{-1} Ω·cm. The sudden drop near 100 °C was attributed to the enhanced chain mobility of the polymer above the glass transition temperature (~100 °C). The nanoparticles could move to the surfaces of the nanofibers due to the phase separation from the polymer matrix. Therefore, the increased population of the nanoparticles on the surface facilitated electrical percolation. The resistivity of the mat after the third reduction cycle decreased from 6.9×10^{-3} to 3.3×10^{-3} Ω·cm at 150 °C, and then saturated at higher annealing temperatures. The sudden drop in the resistivity near 100 °C was not observed in the mats subjected to three reduction cycles. It was regarded that the volume fraction of the Au nanoparticles was high enough before thermal annealing such that the movement of the nanoparticles to the surface did not cause a noticeable change in the resistivity. SEM images in Figure S2 (Supporting Information) show the morphological changes in the Au nanoparticles at annealing temperatures of 110 and 160 °C. Five samples were used for every resistivity measurement.

Conductive micropatterns can find applications either in electric circuits or in strain sensors.[34] Electric circuits require invariance in resistivity under a mechanical strain, while strain sensors require a large variance in resistivity under an external strain. Because the resistivity of the composite mat can be controlled by adjusting the concentration of the precursor

dx.doi.org/10.1021/am4026032 | ACS Appl. Mater. Interfaces 2013, 5, 8766−8771

solution and the number of reduction cycles, the mat can be used for both electric circuits and strain sensors. Figure 6 shows

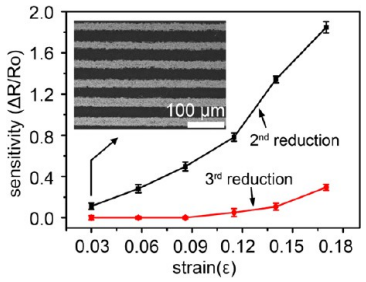

Figure 6. Sensitivity ($\Delta R/R_0$) changes with strain for the 50-μm line-and-space composite pattern obtained after the second and third reduction cycles. The inset SEM image shows the line-and-space pattern of the P4VP/Au composite mat.

the changes in the sensitivity ($\Delta R/R_0$) of a line pattern of the composite mat (width, 50 μm; thickness, 5 μm), as shown in the inset SEM image, fabricated on a 150-μm-thick PET film. R_0 is resistivity without strain and ΔR is defined as ($R - R_0$). The strain ($\varepsilon = h/2r$), where h is the sample thickness and r is the bending radius, was applied with an automatic bending machine (Figures S3 and S4, Supporting Information). Five samples were used for every measurement. In the pattern after the second reduction cycle, the resistivity was sensitive to the strain applied on the substrate. The value of $\Delta R/R_0$ was 0.11 at $\varepsilon = 0.030$ and monotonically increased to 0.78 at $\varepsilon = 0.115$ and 1.87 at $\varepsilon = 0.17$. This sensitivity is very similar to the reported result (2.0 at $\varepsilon = 0.2$) from a Au thin film deposited on a PDMS membrane, in which the Au had an interconnected network structure.[35] The maximum measurable strain was 17% because the substrate was completely bent at this value (Figure S4, Supporting Information). In contrast to the line pattern subjected to two reduction cycles, that subjected to three reduction cycles did not show any response to strain at $\varepsilon = 0.115$. It showed a slight response at higher strain values. The high density of the Au nanoparticles facilitated in maintaining percolation as long as the substrate was not extremely bent.[36] Although the resistivity increased slightly at $\varepsilon = 0.17$, the pattern was still very conductive so that it could be used for electric circuits. In most of the literature on highly flexible conductive circuits,[37−39] some degree of increase (<10%) in resistivity at $\varepsilon = 0.1$ has been reported.

Strain-invariant or strain-sensitive patterns can be employed to fabricate a strain sensor from the composite nanofiber mat only. Figure 7A exhibits the schematic illustration for the process to fabricate the strain sensor. The electrospun fiber mat was exposed to UVO through a line-and-space mask. After dissolving the shielded fibers by dipping the mat in ethanol, a polystyrene (PS) line (width: 160 μm) was drawn by nozzle printing at the center of the fiber mat pattern (Figure 7B). A highly concentrated PS solution (15 wt % in chloroform) was released through a nozzle tip (diameter: 100 μm) under 100 kPa. One reduction cycle was then carried out. After dissolving the PS line with chloroform, two more reduction cycles were carried out to generate a strain-invariant circuit (third reduction) and a strain-sensitive area (second reduction) (Figure 7C). This process provides a simple way to create an array of strain sensors and circuits from a single material. Figure 7D shows the performance of the strain sensor exhibited in Figure 7C in terms of the sensitivity change during the repeated

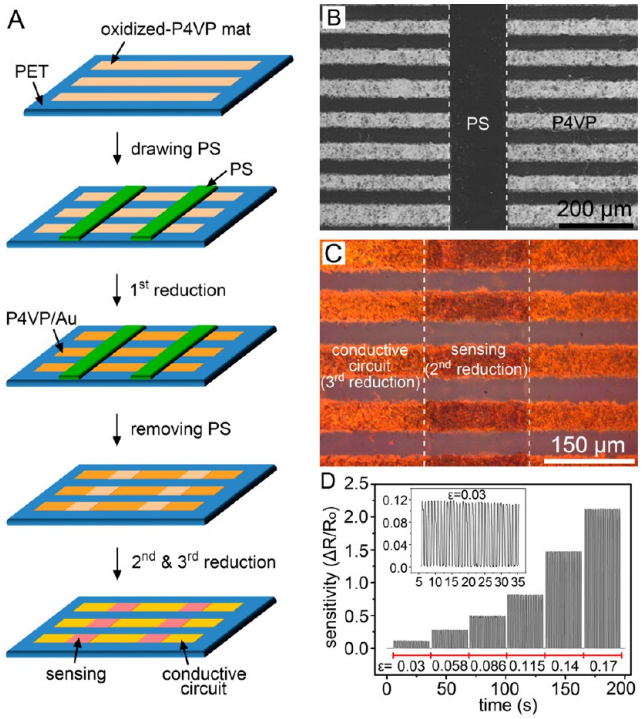

Figure 7. Application of conductive composite nanofibers as a strain sensor. (A) Schematic illustration of overall process fabricating the strain sensor. (B) SEM image of the patterned P4VP mat on which a PS line (width: 160 μm) was drawn by nozzle printing. (C) Optical microscopy image of P4VP/Au composite patterns. After the first reduction, the PS line was dissolved and two more reduction cycles were then carried out. The pattern after the third reduction was strain-invariant and that after the second reduction was sensitive to strain. (D) Real-time sensitivity changes in strain in the range $\varepsilon = 0.03$−0.17. The inset shows a magnified graph for the sensitivity change at $\varepsilon = 0.03$ during 30 cycles.

bending cycles. The measurement was carried out at a frequency of 1 Hz (32 cycles for each strain value in the range 0.03−0.17). The composite nanofiber pattern showed complete stability over 200 bending cycles and recovered the initial resistivity without any mechanical or electrical failure (Figure S5, Supporting Information). The inset in Figure 7D shows a magnified image of the sensitivity profile during the bending cycles at $\varepsilon = 0.03$.

Even though many researches on the strain sensors introduced a variety of fabricating methods and showed high performance (e.g., high sensitivity, steady change of the sensitivity for strains), the promising perspective on the strain sensors is to realize the application to a human skin. Recently, some papers have demonstrated attachable strain sensors on a human body.[4,5,34,40−42] The strain sensors could recognize diverse motions including stretching, twisting, bending, and pressing. Fabricating sensors on a skin-compatible elastomeric thin film is desirable for the wearable strain sensor. The strategy introduced in this work will be combined with the patterned stretchable electrode to generate an array of stretchable sensors to recognize diverse motions and the direction of external stimulation.

CONCLUSION

We demonstrated simple lithographic micropatterning of P4VP/Au composite nanofiber mats and utilized the patterns

for fabricating a strain sensor. P4VP nanofiber micropatterns were obtained through selective UVO exposure of the nanofiber mat followed by dissolving the shielded nanofibers. Au precursors formed a complex with the pyridyl groups of the polymer. Repeated complexation-and-reduction cycles significantly decreased the resistivity of composite fiber mats. The resistivity could be adjusted by controlling the number of reduction cycles and the thickness of the fiber mat. Nozzle-printing was employed to fabricate a strain sensor composed of a strain-sensitive part and strain-invariant circuit. We expect that the strain sensor with high performance will be proposed as another approach to build sensing devices.

■ ASSOCIATED CONTENT

Supporting Information

Digital photos and SEM images of P4VP/Au nanofiber mats, HR-TEM image of Au nanoparticles, digital photos of a bending machine. This material is available free of charge via the Internet at http://pubs.acs.org.

■ AUTHOR INFORMATION

Corresponding Authors

*E-mail: ujeong@yonsei.ac.kr (U.J.).
*E-mail:jongjin00.park@samsung.com (J.P.).

Notes

The authors declare no competing financial interest.

■ ACKNOWLEDGMENTS

This research was supported by a National Research Foundation (NRF) grant funded by the Korean Government (MSIP) through the Active Polymer Center Pattern Integration (No. 2007-0056091) and through the "IT Consilience Creative Program" (NIPA-2013-H0203-13-1001). We thank Dr. Mino Yang at Analytical Science Group of SAIT for STEM analysis.

■ REFERENCES

(1) Rogers, J. A.; Someya, T.; Huang, Y. *Science* **2010**, *327*, 1603−1607.
(2) Kim, D.-H.; Rogers, J. A. *Adv. Mater.* **2008**, *20*, 4887−4892.
(3) Li, X.; Zhang, R.; Yu, W.; Wang, K.; Wei, J.; Wu, D.; Cao, A.; Li, Z.; Cheng, Y.; Zheng, Q.; Ruoff, R. S.; Zhu, H. *Sci. Rep.* **2012**, *2*, 870.
(4) Pang, C.; Lee, G. -Y.; kim, T.; Kim, S. M.; Kim, H. N.; Ahn, S.-H.; Suh, K.-Y. *Nat. Mater.* **2012**, *11*, 795−801.
(5) Yamada, T.; Yamamoto, Y.; Yomogida, Y.; Izadi-Najafabadi, A.; Futaba, D. N.; Hata, K. *Nat. Nanotechnol.* **2011**, *6*, 296−301.
(6) Yu, C.; Wang, Z.; Yu, H.; Jiang, H. *Appl. Phys. Lett.* **2009**, *95*, 141912.
(7) Liu, H.; Kameoka, J.; Czaplewski, D. A.; Craighead, H. G. *Nano Lett.* **2004**, *4*, 671−675.
(8) Hyun, D. C.; Park, M.; Park, C.; Kim, B.; Xia, Y.; Hur, J. H.; Kim, J. M.; Park, J. J.; Jeong, U. *Adv. Mater.* **2011**, *23*, 2946−2950.
(9) Lacour, S. P.; Wagner, S.; Huang, Z.; Suo, Z. *Appl. Phys. Lett.* **2003**, *82*, 2404.
(10) Park, J.; Wang, S.; Li, M.; Ahn, C.; Hyun, J. K.; Kim, D. S.; Kim, D. K.; Rogers, J. A.; Huang, Y.; Jeon, S. *Nat. Commun.* **2012**, *3*, 916.
(11) Yun, S.; Niu, X.; Yu, Z.; Hu, W.; Brochu, P.; Pei, Q. *Adv. Mater.* **2012**, *24*, 1321−1327.
(12) Lee, J.; Lee, P.; Lee, H.; Lee, D.; Lee, S. S.; Ko, S. H. *Nanoscale* **2012**, *4*, 6408−6414.
(13) Zhang, Y.; Sheehan, C. J.; Zhai, J.; Zou, G.; Luo, H.; Xiong, J.; Zhu, Y. T.; Jia, Q. X. *Adv. Mater.* **2010**, *22*, 3027−3031.
(14) Niu, X.; Peng, S.; Liu, L.; Wen, W.; Sheng, P. *Adv. Mater.* **2007**, *19*, 2682−2686.
(15) Park, S.-I.; Xiong, Y.; Kim, R.-H.; Elvikis, P.; Meitl, M.; Kim, D.-H.; Wu, J.; Yoon, J.; Yu, C.-J.; Liu, Z.; Huang, Y.; Hwang, K.-C.; Ferreira, P.; Li, X.; Choquette, K.; Rogers, J. A. *Science* **2009**, *325*, 977−981.
(16) Khang, D.-Y.; Jiang, H.; Huang, Y.; Rogers, J. A. *Science* **2006**, *311*, 208−212.
(17) Park, M.; Im, J.; Shin, M.; Min, Y.; Park, J.; Cho, H.; Park, S.; Shim, M.-B.; Jeon, S.; Chung, D.-Y.; Bae, J.; Park, J.; Jeong, U.; Kim., K. *Nat. Nanotechnol.* **2012**, *7*, 803−809.
(18) Persano, L.; Dagdeviren, C.; Su, Y.; Zhang, Y.; Girado, S.; Pisignano, D.; Huang, Y.; Rogers, J. A. *Nat. Commun.* **2013**, *4*, 1633.
(19) Tiwari, M. K.; Yarin, A. L.; Megaridis, C. M. *J. Appl. Phys.* **2008**, *103*, 044305.
(20) Xiao, X.; Yuan, L.; Zhong, J.; Ding, T.; Liu, Y.; Cai, Z.; Rong, Y.; Han, H.; Zhou, J.; Wang, Z. L. *Adv. Mater.* **2011**, *23*, 5440−5444.
(21) Shi, J.; Wang, L.; Chen, Y. *Langmuir* **2009**, *25*, 6015−6018.
(22) Carlberg, B.; Wang, T.; Liu, J. *Langmuir* **2010**, *26*, 2235−2239.
(23) Li, D.; Ouyang, G.; McCann, J. T.; Xia, Y. *Nano Lett.* **2005**, *5*, 913−916.
(24) Theron, A.; Zussman, E.; Yarin, A. L. *Nanotechnology* **2001**, *12*, 384−390.
(25) MacDiarmid, A. G. *Angew. Chem., Int. Ed.* **2001**, *40*, 2581−2590.
(26) Sun, D.; Chang, C.; Li, S.; Lin, L. *Nano Lett.* **2006**, *6*, 839−842.
(27) Lee, S. W.; Lee, H. J.; Choi, J. H.; Koh, W. G.; Myoung, J. M.; Hur, J. H.; Park, J. J.; Cho, J. H.; Jeong, U. *Nano Lett.* **2010**, *10*, 347−351.
(28) Park, S.; Moon, S. C.; Chen, D.; Farris, R. J.; Russell, T. P. *J. Mater. Chem.* **2010**, *20*, 1198−1202.
(29) Dong, H.; Fey, E.; Gandelman, A.; Jones, W. E., Jr. *Chem. Mater.* **2006**, *18*, 2008−2011.
(30) Menon, V. P.; Martin, C. R. *Anal. Chem.* **1995**, *67*, 1920−1928.
(31) Park, M.; Hyun, D. C.; Kim, J.; Kim, Y. S.; Jeong, U. *Chem. Mater.* **2010**, *22*, 4166−4174.
(32) Park, M.; Xia, Y.; Jeong, U. *Angew. Chem., Int. Ed.* **2011**, *50*, 10977−10980.
(33) Chun, K.-Y.; Oh, Y.; Rho, J.; Ahn, J.-H.; Kim, Y.-J.; Choi, H. R.; Baik, S. *Nat. Nanotechnol.* **2010**, *5*, 853−857.
(34) Lu, N.; Lu, C.; Yang, S.; Rogers, J. *Adv. Funct. Mater.* **2012**, *22*, 4044−4050.
(35) Graz, I. M.; Cotton, D. P. J.; Lacour, S. P. *Appl. Phys. Lett.* **2009**, *94*, 071902.
(36) Ruschau, G. R.; Yoshikawa, S.; Newnham, R. E. *J. Appl. Phys.* **1992**, *72*, 953−959.
(37) Russo, A.; Ahn, B. Y.; Adams, J. J.; Duoss, E. B.; Bernhard, J. T.; Lewis, J. A. *Adv. Mater.* **2011**, *23*, 3426−3430.
(38) Wu, H.; Hu, L.; Rowell, M. W.; Kong, D.; Cha, J. J.; McDonough, J. R.; Zhu, J.; Yang, Y.; McGehee, M. D.; Cui, Y. *Nano Lett.* **2010**, *10*, 4242−4248.
(39) Ahn, B. Y.; Duoss, E. B.; Motala, M. J.; Guo, X.; Park, S.-I.; Xiong, Y.; Yoon, J.; Nuzzo, R. G.; Rogers, J. A.; Lewis, J. A. *Science* **2009**, *323*, 1590−1593.
(40) Kim, D.-H.; Lu, N.; Ma, R.; Kim, Y.-S.; Kim, R.-H.; Wang, S.; Wu, J.; Won, S. M.; Tao, H.; Islam, A.; Yu, K. J.; Kim, T.; Chowdhury, R.; Ying, M.; Xu, L.; Li, M.; Chung, H.-J.; Keum, H.; McCormick, M.; Liu, P.; Zhang, Y. -W.; Omenetto, F. G.; Huang, Y.; Coleman, T.; Rogers, J. A. *Science* **2011**, *333*, 838−843.
(41) Yeo, W.-H.; Kim, Y.-S.; Lee, J.; Ameen, A.; Shi, L.; Li, M.; Wang, S.; Ma, R.; Jin, S. H.; Kang, Z.; Huang, Y.; Rogers, J. A. *Adv. Mater.* **2013**, *25*, 2773−2278.
(42) Bae, S.-H.; Lee, Y.; Sharama, B. K.; Lee, H.-J.; Kim, J.-H.; Ahn, J.-H. *Carbon* **2013**, *51*, 236−242.